A Barrel-Shaped Metal–Organic Blue-Box Analogue with Photo-/Redox-Switchable Behavior

Gabriel Brunet, Elizaveta Suturina, Guillaume George, Jeffrey Ovens, Paul Richardson, Christophe Bucher, Muralee Murugesu

A Barrel-Shaped Metal-Organic Blue-Box Analog with Photo-/Redox-Switchable Behavior

Gabriel Brunet,[a] Elizaveta A. Suturina,[b] Guillaume P. C. George,[c] Jeffrey S. Ovens,[a] Christophe Bucher*[c] and Muralee Murugesu*[a]

[a] Department of Chemistry and Biomolecular Sciences, University of Ottawa, 10 Marie Curie, Ottawa, ON, K1N 6N5, Canada.
[b] Department of Chemistry, University of Bath, Claverton Down, Bath, BA2 7AY, UK.
[c] Univ. Lyon, ENS de Lyon, CNRS UMR 5182, Université Claude Bernard Lyon 1, Laboratoire de Chimie, F69342, Lyon, France.

Donor acceptor interactions are ubiquitous in the design and understanding of host-guest complexes. Despite their non-covalent nature, they can readily dictate the self-assembly of complex architectures. Here, we present a photo-/redox-switchable metal-organic nanocapsule, assembled using lanthanide ions and viologen building blocks, that relies on such donor-acceptor interactions. We highlight the potential of this unique barrel-shaped structure for the encapsulation of suitable electron donors, akin to the well-investigated "blue-box" macrocycles. The light-triggered reduction of the viologen units has been investigated by single-crystal-to-single-crystal X-ray diffraction experiments, complemented by magnetic, optical and solid-state electrochemical characterizations. Density functional theory (DFT) calculations were employed to suggest the most likely electron donor in the light-triggered reduction of the viologen-based ligand.

Introduction

The biology of living systems provides some of the most complex, yet efficient examples of how external stimuli can be used to trigger desired responses. Such cause and effect mechanisms rely on critical changes that occur at the molecular-scale, as a result of variations in external factors such as temperature, pressure or pH. In this regard, large polynuclear metal clusters have attracted significant attention over the last few years, due to their structural similarities to biologically active sites that control physiological responses.[1-3] The design of stimuli-responsive metal-organic supramolecular architectures has recently become a highly desirable,[4-15] yet challenging task, in part due to the ability to establish key structure-property relationships, useful to the development of biomimetic systems. More importantly, such molecules offer the potential to provide access to "smart" molecular materials with increased functionality and utility in a variety of different fields, including that of catalysis,[16,17] magnetism,[18-21] sensing and electronics.[22-25]

The bottom-up strategy that we have been exploring over the past few years to gain access to stimuli-responsive functional metal-organic assemblies hinges on the design and implementation of advanced building blocks with enhanced size and complexity.[26-31] In line with these ambitious objectives, we are now reporting on our approach towards discrete photo-/redox-responsive metal-organic nanocapsules built from lanthanide ions and 4,4'-bipyridinium-based organic linkers. Our main goal here was to achieve a directed assembly of two lanthanide ions, selected for their large radius and high coordination numbers (≥8), with four stimuli-responsive electron-poor bridging organic ligands, so as to provide access to discrete cavitand-like structures with unique magnetic and/or molecular recognition properties. We anticipated that such metal-organic barrel-shaped structures could prove useful either as key precursors in the formation of larger polymeric assemblies or as discrete compounds, to achieve a redox-controlled encapsulation of electron-rich guests. In addition, this strategy could potentially enable the investigation of magnetic entanglement effects between two lanthanide ions mediated by redox-active ligands.[32-35] Along the same lines, the redox-controlled encapsulation of different guest molecules could also play a key role in defining the magnetic characteristics of the complex.

The 4,4'-bipyridinium-based organic linkers, better known as viologens ($\mathbf{V}^{2+}$), have been selected for their remarkable and well-defined redox-activity, wherein two consecutive Nernstian electron transfer processes can occur, leading to the successive formation of a radical-cation ($\mathbf{V}^{+\bullet}$), and a neutral quinonic species ($\mathbf{V}^{0}$).[36-40] Further attractive features of viologen-based ligands include an outstanding stability of the cation radical state ($\mathbf{V}^{+\bullet}$) and an ability of most electron-acceptor $\mathbf{V}^{2+}$ derivatives to form stable charge transfer complexes with a wide range of electron donors.[41,42]

One of the most well-known representative examples of this class of compound is the so-called "blue box" macrocycle, that features two viologen units held in a cofacial arrangement through paraxylene linkers. The prominence of such molecular arrangements is closely tied to Stoddart's achievements in the field of molecular machines and mechanically interlocked molecules.[43,44]

Building upon our previous achievements on air-stable radical-bridged complexes for probing magnetic exchange interactions,[34,45,45] we sought to devise a series of functional metal-organic architectures incorporating stimuli-responsive organic linkers displaying at least two accessible/stable redox states. Our efforts have focused on 1,1'-bis(4-carboxyphenyl)-(4,4'bipyridinium) dichloride (H_2bcbp·2Cl), featuring two coordinating carboxylate moieties at each end of the molecule, to promote either the formation of high dimensionality coordination networks or extended nanocapsules upon metal coordination. As part of these ongoing efforts, we found that this rigid viologen-based ligand reacts with Dy^{III} cations to yield the discrete and highly symmetrical viologen-based metal-organic assembly $[Dy_2(bcbp)_4(H_2O)_8]Cl_6·H_2O$ (**1**) depicted in Fig. 1.

Results and discussion

Structural details

The complex **1** was synthesized by reacting $Dy(NO_3)_3·6H_2O$ with $(H_2bcbp)Cl_2$ in a solvent mixture of DMF/MeCN/H_2O under slightly acidic solvothermal conditions. The resulting yellow plate monocrystals (Fig. S1) were isolated after slow cooling. The molecular structure, determined by single-crystal X-ray diffraction (Table S1), belongs to the tetragonal *I*4/*m* space group and reveals an unprecedented barrel-shaped nanocapsular arrangement. The staves of the barrel are represented by four bent $bcbp^{2-}$ ligands, the heads are comprised of two crystallographically equivalent Dy^{III} ions separated by 21.44 Å, and the hoops can be thought of the carboxylic acid moieties (Fig. 2). The charge of each discrete cationic $[M_2L_4]^{6+}$ barrel is balanced by six chloride anions; two of them (Cl2 and Cl3) are confined within the molecular cage (Fig. 2C), while another is found between the barrels (Cl1). The remaining Cl^- anions are generated by symmetry operations within the molecule. Each Dy^{III} ion is coordinated by 8 oxygen atoms brought by 4 carboxylate moieties and by 4 water molecules acting as stoppers at both ends of the assembly.

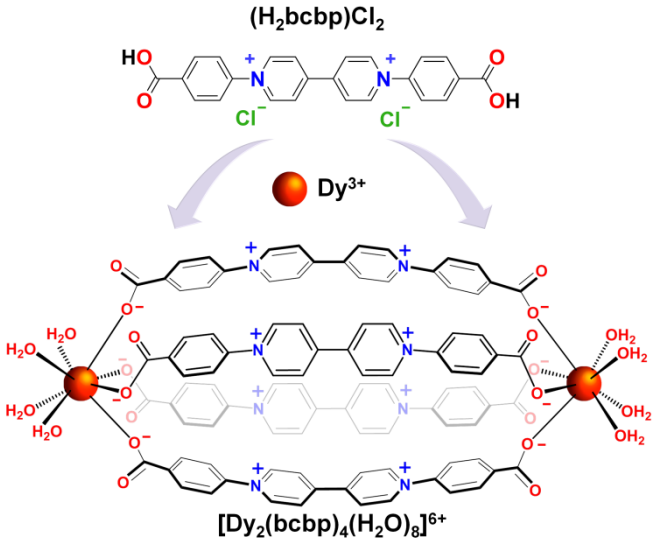

Fig. 1 Schematic representation of the $(H_2bcbp)^{2+}$ ligand and of the title barrel-shaped dysprosium-viologen assembly.

At first glance, due to the four-fold symmetry of the complex, a nearly perfect square antiprismatic (SAP) geometry is observed, with angles within each square equal to the ideal 45°. The coordination sphere of the lanthanide ion was then investigated by SHAPE analysis, revealing a slightly distorted SAP geometry (Table S2).[47] Upon further inspection, the distortion is induced by a slight contraction of the SAP environment, highlighted by the distance between the upper and lower planes containing the four oxygen atoms (d_{pp} = 2.47 Å) and the average distance between the oxygen atoms within each plane (d_{in} = 2.89 Å). Such deviations from an ideal D_{4d} symmetry are expected to have a significant impact on the slow magnetic relaxation dynamics of the Dy^{III} ions (*vide infra*). In addition to the aforementioned four-fold symmetry, there is an inversion centre that lies in the middle of the void space of the capsule, making the overall structure highly symmetrical in nature. The internal area of **1** has been estimated using the SQUEEZE routine of PLATON,[48] revealing a void space of approximately 159 $Å^3$ and containing 64 electrons. These numbers are in agreement with the structural model in which a total of two Cl^- anions and two H_2O molecules can be encapsulated simultaneously within the nanocapsule. The Cl^- anions occupy two distinct positions within the capsule (Cl2 and Cl3) and the shortest distance measured between the center of a pyridinium ring and an offset chloride anion (Cl3)

reaches 3.54 Å. This value is consistent with other viologen-halide distances found in literature.[49-53] On the other hand, the Cl_2 atom is found lying at the centre of the capsule, at an equal distance (4.24 Å) to all viologen ligands. It appears that the cavity of **1** is ideally suited to Cl^-; all attempts to synthesize the Br^- and I^- analogs were unsuccessful. This may be due to size constraints within the capsule as we move towards larger halides (ionic radii of 1.67, 1.82 and 2.06 Å, for Cl^-, Br^- and I^-, respectively). On a larger scale, each of the nanocapsules are aligned parallel to one another, separated by a network of Cl^- anions. The nearest intercapsular Dy–Dy distance is 7.86 Å, where terminally coordinated H_2O molecules exhibit van der Waals and hydrogen-bonding interactions with the Cl^- anions to fill the gaps between the lanthanide ions (Fig. S2).

Reduction of the nanobarrel

The presence of four viologen-based ligands led us to explore the redox properties of **1**. We found that viologen radicals (**$V^{+\bullet}$**) can be generated post-synthetically, within the crystal, in response to different environmental stimuli such as light, temperature or to selected chemical reducing agents. In all cases, the formation of **$V^{+\bullet}$** was easily revealed by a drastic color change of the single crystals, going from yellow to green, upon application of external stimuli (Fig. 3). The use of heat or chemical reducing agents, such as sodium dithionite, was found to trigger this change in color; however, this was unfortunately also accompanied by a loss in crystallinity of the single-crystals. On the other hand, when subjected to UV irradiation, the single-crystals retained crystallinity allowing for single-crystal-to-single-crystal X-ray diffraction measurements

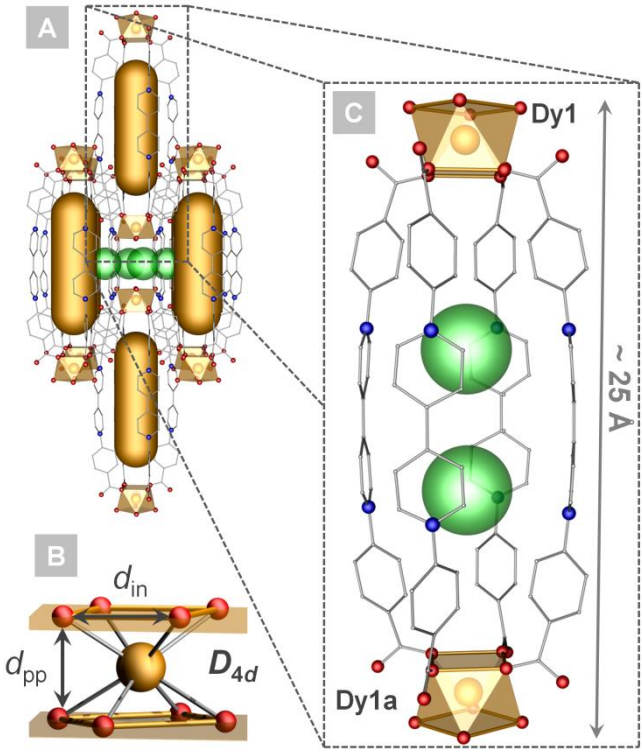

Fig. 2 (A) Packing arrangement of **1** along the *a*-axis, highlighting the cylindrical void space of the nanocapsule. (B) The square antiprismatic geometry of the Dy^{III} ions is shown alongside the molecular structure of the nanobarrel displaying encapsulated chloride anions (C). Selected chloride counter-anions, uncoordinated water molecules and hydrogen atoms have been omitted for clarity. Color code: Dy^{III}–orange, Cl-green, O-red, N-blue, and C-gray vertices.

to be carried out, while also displaying a similar change in color (Fig. 3). The more mild nature of UV irradiation, compared to chemical reduction or heat, allows the retention of crystallinity, even if less radicals are likely to be generated.[54,55] The structures of the photochemically reduced nanocapsules, wherein at least part of the **V^{2+}** units have been converted into the one electron reduced **$V^{+\bullet}$** have been retained, yet examination of some key bond lengths suggests the presence of viologen-based radicals (Fig. 3). To further confirm this, we have synthesized the diamagnetic yttrium analog (**2**), whose solid-state structure was identical to that of **1** (Table S1). The reduced structures of both Dy^{III} (**1'**) and Y^{III} (**2'**) analogs have been successfully elucidated using this strategy.

The maximum number of **$V^{+\bullet}$** species generated per capsule will in any case be limited by the number of electron donors available in the sample (possible mechanisms are discussed in the following section). These restrictions, taken together with the experimental

data collected for **1'** and **2'**, led us to the conclusion that only a limited proportion of viologens end up being reduced in the crystals, as observed in other similar photoreduced systems.[54,55] The X-ray data collected after irradiation thus correspond to an average picture taking into account the ratio between reduced and non reduced viologens in the four-order symmetry barrel-shaped structures. Still, we found that irradiation of **2** results in a slight shortening of the central C-C bond length from 1.49(7) to 1.45(6) Å. A shorter distance is a diagnostic feature of viologen radicals due to the delocalization of the single electron over both pyridinium rings.[56,57] The crystal structure of **1** before and after irradiation features almost the same central C-C bond length of 1.55(4) to 1.54(5) Å, respectively. There is also a pronounced shortening of the non-coordinated C-O bond length in the carboxylate fragment upon irradiation, from 1.26(2) Å to 1.204(17) Å in **2**, and 1.237(9) to 1.211(9) Å in **1**, as well as shortening of the C-COO$^-$ bond from 1.55(4) to 1.52(3) Å in **2**, and 1.53(2) to 1.47(2) in **1**. These changes contribute to a slight contraction of the unit cell dimensions along the *a*- and *b*-axes (from 12.72 to 12.58 Å in **1** and from 12.51 to 12.50 Å in **2**), as well as along the *c*-axis (from 29.30 to 28.99 Å in **1**, and from 29.03 to 28.79 Å in **2**). The contraction along the *a*- and *b*-axes in **1** is in part associated with closer interactions between non-encapsulated Cl$^-$ anions (Cl1) and the middle C atom of the ligand (changing from 3.60 to 3.57 Å), while it does not vary significantly in **2**. The distance between the encapsulated Cl$^-$ anions (Cl3) and the pyridinium ring also shortens from 3.54 to 3.47 Å in **1**, and 3.54 to 3.53 Å in **2**.

To unequivocally confirm the presence of organic radicals within the crystals, we collected room-temperature electron paramagnetic resonance (EPR) spectra of the as-synthesized (**1** and **2**) and reduced capsules (**1'** and **2'**). The EPR spectra of the photochemically reduced compounds display a signal centered at g = 2.0025, consistent with the presence of viologen-based radicals (Fig. 4A and Fig. S3).

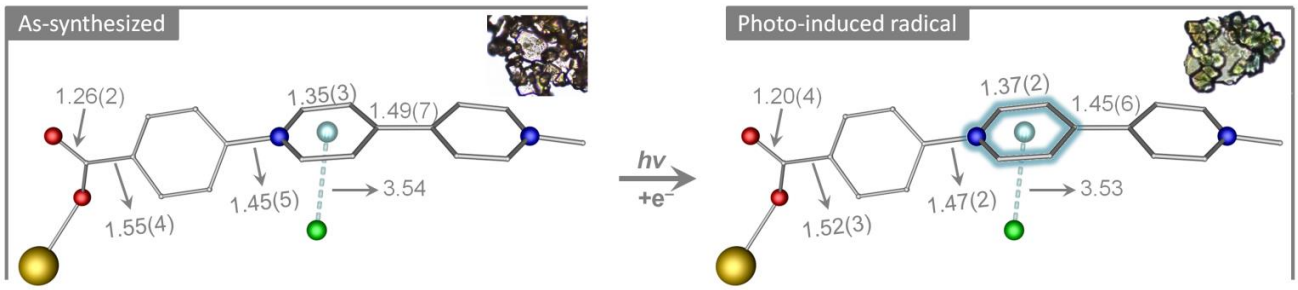

Fig. 3 Comparison of the bond distances found in the as-synthesized and radical form of the viologen ligand in compounds **2** and **2'**, respectively. Optical microscopy pictures display the change in color of the crystals upon UV irradiation. Bond distances are denoted in Ångtröms. Color code: N-blue, Cl-green, Dy-yellow, O-red and C-gray vertices.

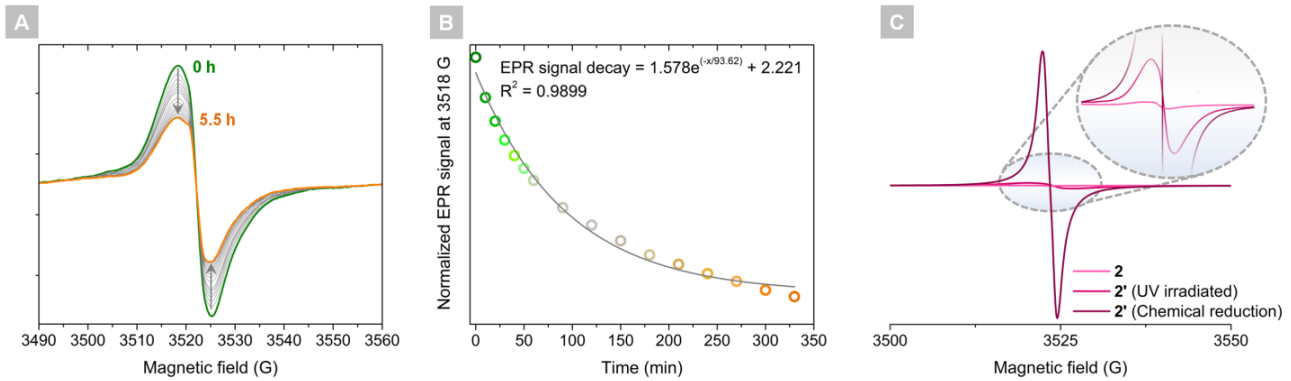

Fig. 4 (A) Time-dependent EPR data of a UV irradiated sample of **2**, measured over 5.5 hours at room temperature, revealing the gradual loss of photogenerated radicals over time. (B) The kinetics of this process can be described by a first-order exponential decay function. (C) Comparison of the EPR signal obtained from the as-synthesized, UV irradiated and chemically reduced nanocapsules.

Interestingly, the use of a chemical reducing agent yields a much stronger EPR signal, while maintaining an identical g value (Fig. 4C). This provides some insight into the number of radicals being generated when reducing

the nanocapsules through either UV irradiation or chemical reduction. While the EPR signal is drastically enhanced following chemical reduction, this process results in significant cracking and loss of crystallinity in the single-crystals, precluding single-crystal-to-single-crystal studies. The as-synthesized compounds also display an EPR signal, albeit much weaker than the irradiated samples, and is nearly impossible to distinguish when compared to the chemically reduced compound, suggesting that ambient UV light likely reduces the structures of **1** and **2**. To investigate the stability of the photo-induced radicals, time-dependent EPR spectra were collected on **2'** over a period of 5.5 hours. We observe a clear decrease in the EPR signal over time, indicating the reversibility of the reduction process (Fig. 4A). The kinetics of this process was studied by examining the EPR signal at 3518 G, from which a first-order exponential equation was found to suitably reproduce the data (Fig. 4B). Alternatively, the slow decrease in the EPR signal may also be caused by the re-oxidation of the viologen radicals by molecular oxygen from the atmosphere, rather than from a back electron transfer reaction to the original donor.

Mechanism of radical formation

There are two possible explanations for the observed photochromic behavior: (i) intermolecular electron transfer (from either Cl^- or H_2O) that changes the total charge of the ligand from 0 to -1, yielding $\mathbf{V^{+\bullet}}$ radical cations,[50,56] or (ii) intramolecular electron transfer from the carboxylic acid to the viologen moiety, resulting in a neutral bcbp ligand with two radical centres (one on the carboxylic acid, **COO$^\bullet$**, and one on the pyridinium moiety, $\mathbf{V^{+\bullet}}$).[57] The former situation leads to spin density only on the pyridinium group, while the latter yields spin density on both the carboxylic acid and pyridinium groups, given the fact that two radical sites per ligand would be formed. Density functional theory (DFT) calculations carried out on the singlet and triplet states of the neutral bcbp ligand with a $\mathbf{V^{2+}}$ fragment, as well as the reduced $bcbp^{-\bullet}$ ligand show that both reduced and triplet states adopt shorter central C-C bonds than $\mathbf{V^{2+}}$ in the singlet state. However, the C-COO^- bond gets shorter in the triplet state, while reduction leads to its elongation (Fig. S4).

Spin density distribution highlights the difference between two scenarios: in the case of an intermolecular electron transfer leading to the formation of a $\mathbf{V^{+\bullet}}$ radical-containing species, the spin density is localized almost solely on the viologen fragment, whereas the triplet state of the neutral ligand features spin density on both the carboxylate and the bypiridinium fragments (Fig. 5). It appears to be very difficult to unambiguously state whether the radical formation on the viologen fragments are associated to an intermolecular reduction mechanism or if it is a result of excitation to the triplet state of the ligand, as no information on the carboxylate group spin density is available from the experiment. In an attempt to test whether the encapsulated Cl^- anions or water molecules are likely to reduce the capsule, the lowest energy triplet and quintet states of the $[H_2O,Cl_2@[Y_2(bcbp)_4(H_2O)_8]]^{4+}$ complex were optimized using the HF-3c method in ORCA.[59,60] Mulliken spin population of the encapsulated Cl^- and H_2O molecules is close to zero in both cases, suggesting that at first

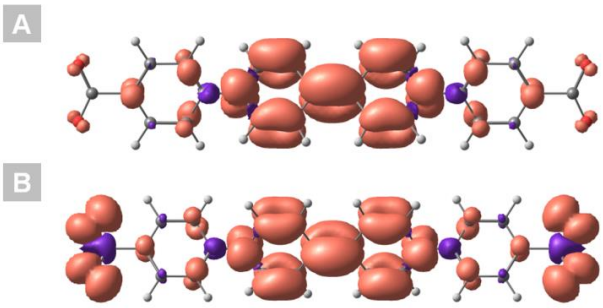

Fig. 5 Spin density distribution plotted with contour value 0.001 for optimised (B3LYP/6-31+G*) $\mathbf{V^{+\bullet}}$ radical cation with an intermolecular electron donor (A) and $\mathbf{V^{+\bullet}}$ radical cation with intramolecular carboxylate donor in the triplet state (B).

instance, the carboxylate groups are likely to act as electron donors rather than the encapsulated Cl^- anions. Nevertheless, previous studies have established the ability of halides to act as electron donors for viologen-based ligands.[49,61,62] It is also interesting to note that despite the higher electronegativity of Cl compared to Br and I, they may provide more stable excited-state species. An extended model, where intermolecular Cl^- anions are also considered (Fig. S5), indicates that the lowest triplet state of the capsule corresponds to the formation of intercapsular $Cl^\bullet$ radicals and $\mathbf{V^{+\bullet}}$. The reactivity of these radicals is the subject of further computational studies.

Diffuse reflectance spectroscopy

The color change associated with the formation of a viologen radical species can be easily monitored by the naked eye. The solid-state diffuse reflectance spectra of **1** in the UV-vis-NIR range shows characteristic bands attributed to the presence of Dy^{III} ions and are a result of Laporte forbidden *f-f* transitions. The bands centered at 1294 and 960 nm can be assigned to the transitions between the $^6H_{9/2}\leftarrow{}^6H_{15/2}$ and $^6H_{5/2}\leftarrow{}^6H_{15/2}$ states, while the 1102 nm band is a combination of the transitions between the $^6H_{7/2}\leftarrow{}^6H_{15/2}$, $^6F_{11/2}\leftarrow{}^6H_{15/2}$ and $^6H_{9/2}\leftarrow{}^6H_{15/2}$ manifolds. Importantly, the reduction of **1** by UV light results in the formation of an intense broad band in the visible range (600-800 nm) that features noticeable vibronic progression with a separation of ~1500 cm^{-1}, characteristic of double C-C bond stretching coupled to electronic transitions. Such a feature is reflective of an electron-transfer interaction from an electron donor to the pyridinium moiety of the viologen ligand (Fig. S6). A similar behavior is observed for **2** and **2'**, at the exception of the noted *f-f* transitions (Fig. S6).

Magnetic behaviour

Given the success of SAP chemical environments for the generation of high performance single-molecule magnets (SMMs),[63-65] we sought to explore the magnetic response of compounds **1** and **1'**. The D_{4d} symmetry is particularly attractive due to the fact that it can minimize transverse crystal-field effects and suppress quantum tunneling of the magnetization – a major hurdle to overcome in the design of lanthanide-based SMMs. While this approach has been mainly applied to Tb^{III}-based double-decker compounds,[62,64] a few Dy^{III} compounds with D_{4d} symmetry have also been shown to display SMM behavior.[66,67] As such, both samples were characterized in the solid-state by static (dc) and dynamic (ac) magnetization measurements. We found that the magnetic data for **1'** is identical to that of **1**, likely indicating that only a small ratio of the bipyridinium cations become radicals under UV irradiation, as stated above. This was further confirmed by our attempts to measure the organic radicals in **2'** which yielded a diamagnetic signal in the superconducting quantum interference device (SQUID) magnetometer, despite the small EPR signal. Consequently, only the magnetic data for **1** will be presented hereafter. The room temperature χT product, measured under an applied field of 1000 Oe, is 28.79 cm^3 K mol^{-1}, which is in strong agreement with the predicted value of 28.34 cm^3 K mol^{-1} for two isolated Dy^{III} ions (Fig. S7). The decrease in the χT value at low temperatures is likely due to the thermal depopulation of the crystal-field split M_J levels and/or magnetic anisotropy. At the same time, *M vs. H* and *M vs.* HT^{-1} plots are consistent with what would be expected for weakly coupled anisotropic Dy^{III} ions (Fig. S8). Ac magnetic susceptibility measurements were also performed to determine the slow magnetic relaxation dynamics and possible SMM behavior. An ac signal was only observed by the application of an external dc field. Consequently, the influence of the field and temperature on the magnetic relaxation times was evaluated by fitting the ac susceptibility data to a generalized Debye model (Fig. S9A and Fig. S10A). In both cases, a suitable fit was obtained by considering only Raman and quantum tunneling of the magnetization (QTM) mechanisms (Fig. S9B and Fig. S10B). The slight structural distortions of the SAP geometry are likely the cause of the rather poor SMM behavior, since ideal D_{4d} symmetries are expected to yield longer relaxation times and significant energy barriers.

To complement the magnetic studies, *ab initio* ligand field analyses were performed (Fig. S11), indicating that the sign of the main ligand field parameter, B_0^2, is negative, unlike those in high performing Dy^{III}-based SMMs (Fig. S12).[68,69] This is consistent with the simple point charge model given that the polar angle of donor atoms (60º) is larger than the magic angle of 54.7º. Consequently, the Kramers doublet (KD) with the largest magnetic moment is destabilized, while the KD with $|M_J| = 0.3\ \mu_B$ and easy-plane like anisotropy g_{eff} = (0.5, 10, 10) is stabilized. The first excited state is located only 5 cm^{-1} above the ground state (Table S3), which is consistent with the dominant Raman and QTM type of relaxation found in the ac experiments (see Supplementary Information for more details).

Electrochemistry

To further examine the redox behavior of the nanocapsules, we have performed the electrochemical

characterization of **1** in the solid state using Nafion as a negatively charged conducting matrix. The cyclic voltammogram depicted in Fig. 6A has been recorded at a vitreous carbon electrode modified with a finely grinded mixture of **1** and Nafion. The presence of dicationic viologen units in the capsule is confirmed by the observation of two reduction waves at $(E_{pc})_1$ = –0.35 V and $(E_{pc})_2$ = –0.6 V attributed to the successive formation of $\mathbf{V}^{+\bullet}$ and $\mathbf{V}^0$.

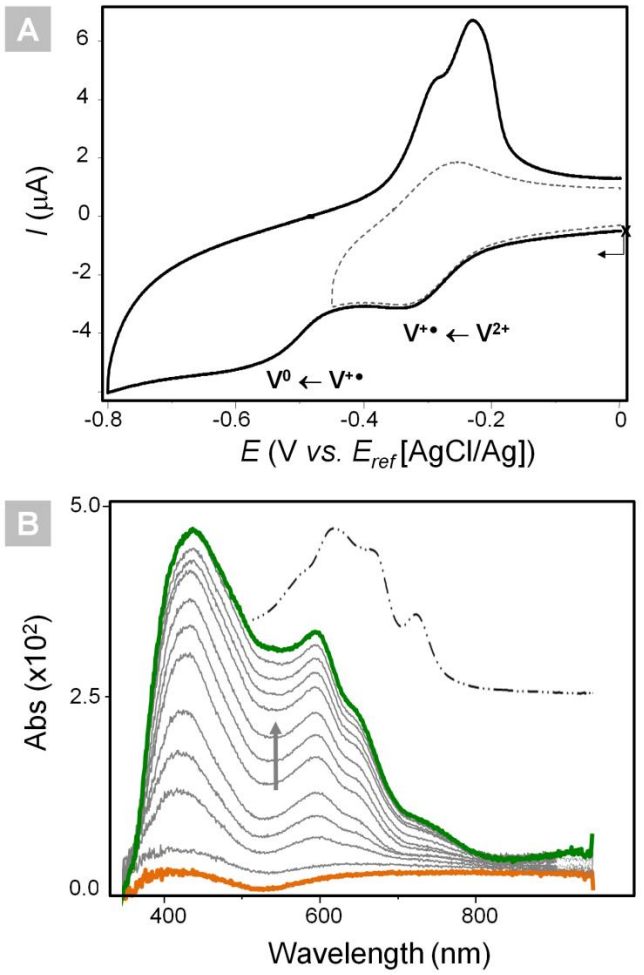

Fig. 6 (A) Solid-state CV curve recorded with a vitreous carbon electrode modified with a **1**/Nafion mixture (Ø 2mm, 50 mV/s) displaying the successive reduction waves attributed to the formation of $\mathbf{V}^{+\bullet}$ and $\mathbf{V}^0$. (B) *In situ* solid-state UV-vis-NIR spectroelectrochemical data recorded upon submitting a **1**/Nafion modified FTO electrode to a potentiostatic reduction at E_{app} = –0.45 V. The changes reveal the color progression from yellow to green associated to the formation of viologen radical species within the nanocapsule. For comparison, the absorption spectrum of a reference compound generated in solution, the cation radical of 1,1'-dimethyl-4,4'-bipyridinium, is shown in the dashed line.

The observation of Gaussian-shaped reoxidation peaks associated with the reduction of $\mathbf{V}^{+\bullet}$ at $(E_{pc})_2$ = –0.6 V suggests the existence of adsorption phenomena involving the neutral quinonic $\mathbf{V}^0$ species. The attribution of the first reduction wave to the one-electron reduction of $\mathbf{V}^{2+} \rightarrow \mathbf{V}^{+\bullet}$ could be further confirmed by spectroelectrochemistry experiments which involved regularly recording absorption spectra over time during the potentiostatic reduction of a fluoride-doped indium-tin oxide transparent electrodes (FTO) modified with a mixture of **1** in Nafion (Fig. 6B). The electrolysis carried out at E_{app} = –0.45 V led to the emergence of a series of bands in the visible range (400/800 nm) including a diagnostic signal centered at 600 nm, associated to a few shoulders between 600 and 800 nm, attributed to the one-electron reduction of all the $\mathbf{V}^{2+}$ units within the capsule. The absence of signals in the near-infrared region also supports the conclusion that the viologen cation radicals are too distant to interact through space, a result which is consistent with a distance of 4.93 Å measured in the solid state.

Conclusions

Viologen-based complexes have a remarkable ability to undergo reversible electron transfer reactions under a variety of stimuli. In such cases, the chemical environment surrounding the viologen group is crucial to generating radical species. Indeed, the presence of a suitable electron donor residing near the pyridinium ring is the determining factor in whether two redox states can be achieved. While no requirement has been clearly established in terms of minimum distance between donor and acceptor atoms, it is generally accepted that a distance in the 3.50 Å range is required to enable an intermolecular electron transfer in the solid-state.[70,71] As such, it is easy to envision how external stimuli, such as pressure, temperature, or even hydration levels, could play a key role in providing the required threshold for radical formation. Although nearly 150 lanthanide compounds coordinated to viologen linkers have been synthesized, only a select few (~5) have been shown to enable the formation of a radical species.[70,72-75] This illustrates the difficulty in promoting supramolecular arrangements that favor electron transfer processes. Among the few compounds that display a viologen-based photo-activated electron transfer, the majority forego a proper identification of the electron donating species. In fact, to this day, the mechanism of formation for such radical-based intermediates remains speculative. At the current stage, we cannot entirely rule

out any possible electron donation mechanisms arising from potential nearby intra- or intermolecular donors. Another scenario already mentioned in the literature involves photoionization of a viologen unit to form V^{3+} and subsequent generation of $V^{+\bullet}$ and V^{2+} species.[76] This process would then rely entirely upon an electron transfer between the viologen ligands themselves. We can, however, rule out the possibility of radicals interacting through space between two capsules (*vide supra*). With this in mind, the generation of $Cl^{\bullet}$ species is to be expected should the Cl^- anions act as donor atoms. Such species are highly reactive and short-lived, which makes reversibility of this process highly unlikely. Attempts to observe $Cl^{\bullet}$ species within their expected range in the EPR spectra has so far been unsuccessful.

To summarize, a new nanocapsular arrangement has been achieved using viologen building blocks and lanthanide ions. The complex exhibits an impressive multi-stimuli responsive behavior where reduction of the viologen ligand can be accessed by three different means: light, chemical reduction, and temperature. The photo-induced radical-bearing nanobarrel has been comprehensively characterized and probed by DFT calculations in order to elucidate the most likely electron donor responsible for the redox behavior. The presence of radical species within the nanocapsule has been confirmed by EPR, diffuse reflectance spectroscopy, and by electrochemical means. Such synthetic approaches should assist in the design of new and efficient molecules that can be utilized in light harvesting and thermal sensing devices, as we extend the richness of organic donor-acceptor materials towards discrete metal-organic cages.

Experimental section

Unless otherwise stated, all materials were commercially available and used without further purification. All solvents were of analytical grade and use without further purification. $Dy(NO_3)_3{\cdot}6H_2O$ and $Y(NO_3)_3{\cdot}6H_2O$ were purchased from Strem Chemicals. 1-chloro-2,4-dinitrobenzene and 4,4'-bipyridine were purchased from Alfa Aesar. Hydrochloric acid (~38%) and other solvents were purchased from Fisher Scientific. All compounds were obtained through solvothermal synthesis and characterized by single-crystal X-ray diffraction studies. Additional experimental details can be found in the Supplementary Information.

Synthesis of 1,1'-bis(4-carboxyphenyl)-(4,4'bipyridinium) dichloride (H_2bpcp·2Cl)

The ligand was synthesized in accordance with previously described procedures.[77]

Synthesis of $[Dy_2(bpcp)_4(H_2O)_8]Cl_6{\cdot}H_2O$ (1)

Compound **1** was synthesized by combining $Dy(NO_3)_3{\cdot}6H_2O$ (11.5 mg; 0.025 mmol) and H_2bpcp·2Cl (20 mg; 0.05 mmol) in a solvent mixture consisting of 2 mL of DMF, 0.5 mL of MeCN and 0.5 mL of H_2O. The resulting solution was placed in a 20 mL scintillation vial and 23 µL of concentrated HCl (37%) were added. Following 10 min of sonication, the vial was heated to 80 °C for 36 hours and cooled to room temperature over an additional 15 hours, yielding phase pure yellow plate crystals. Yield = 34.9 %. Elemental analysis found (calcd) for $C_{96}H_{92}Cl_6Dy_2N_8O_{25}$: C 49.89 (50.23) %, H 3.92 (4.04)%, N 5.19 (4.88)%. Selected IR (solid, cm^{-1}): 3270 (br), 3110 (w), 3031 (m), 1602 (s), 1549 (s), 1497 (w), 1441 (w), 1386 (s), 1252 (m), 1230 (m), 1175 (w), 1101 (w), 1021 (w), 840 (s), 784 (s), 701 (s), 644 (s).

Synthesis of $[Y_2(bpcp)_4(H_2O)_8]Cl_6{\cdot}H_2O$ (2)

Compound **2** was synthesized by combining $Y(NO_3)_3{\cdot}6H_2O$ (9.6 mg; 0.025 mmol) and H_2bpcp·2Cl (20 mg; 0.05 mmol) in a solvent mixture consisting of 2 mL of DMF, 0.5 mL of MeCN and 0.5 mL of H_2O. The resulting solution was placed in a 20 mL scintillation vial and 23 µL of concentrated HCl (37%) were added. Following 10 min of sonication, the vial was heated to 80 °C for 36 hours and cooled to room temperature over an additional 15 hours, yielding phase pure yellow plate crystals. Yield = 36.4 %. Elemental analysis found (calcd) for $C_{96}H_{92}Cl_6Y_2N_8O_{25}$: C 53.38 (53.67) %, H 4.01 (4.32)%, N 5.57 (5.22)%. Selected IR (solid, cm^{-1}): 3246 (br), 3110 (w), 3028 (m), 1603 (s), 1551 (s), 1497 (w), 1442 (w), 1386 (s), 1252 (m), 1230 (m), 1175 (w), 1101 (w), 1021 (w), 840 (s), 784 (s), 701 (s), 645 (s).

Synthesis of reduced compounds (1' and 2')

The isolation of the reduced compounds can be obtained in three different ways: UV-irradiation, heating and chemical reduction. The reduction using light was performed by exposing single-crystals of **1** to four UV lamps of 5 W at a wavelength of 390 nm for one hour. Reduction of **1** by heat was carried out by heating the compound in the solid-state to 80 °C for 3 hours. The chemical reduction of **1** (50 mg) can also be achieved by suspending the complex in a 10 mL solution of 0.0287 mM sodium dithionite in H_2O. It should be noted that the photoreduced compound will slowly revert back to yellow within 48 hours. Given the retention of crystallinity in the UV irradiated samples, we have focused on this specific stimulus to describe the viologen reduction behavior.

Conflicts of interest

There are no conflicts to declare.

Acknowledgements

This work was supported by NSERC (Discovery and DND Discovery Grant), the University of Ottawa and ENS Lyon. We acknowledge the financial support of LIA FunCat in establishing a strong collaboration between the University of Ottawa and ENS Lyon. G. B. gratefully acknowledges the financial support from NSERC (CGS-D and CGS-MSFSS). The authors are also thankful to Paul Richardson for assistance with the EPR measurements.

Notes and references

J. Esselborn, C. Lambertz, A. Adamska-Venkatesh, T. Simmons, G. Berggren, J. Noth, J. Siebel, A. Hemschemeier, V. Artero, E. Reijerse, M. Fontecave, W. Lubitz and T. Happe, *Nat. Chem. Biol.,* 2013, **9**, 607-609.

J. D. Lawrence, H. Li, T. B. Rauchfuss, M. Bénard and M.-M. Rohmer, *Angew. Chem. Int. Ed.,* 2011, **40**, 1768-1771.

E. Salvadeo, L. Dubois and J.-M. Latour, *Coord. Chem. Rev.,* 2018, **374**, 345-375.

A. J. McConnell, C. S. Wood, P. P. Neelakandan and J. Nitschke, *Chem. Rev.,* 2015, **115**, 7729-7793.

M. Han, R. Michel, B. He, Y.-S. Chen, D. Stalke, M. John and G. H. Clever, *Angew. Chem. Int. Ed.*, 2013, **52**, 1319-1323.

P. J. Lusby, P. Müller, S. J. Pike and A. M. Z. Slawin, *J. Am. Chem. Soc.,* 2009, **131**, 16398-16400.

D. S. Kim, J. Chang, S. Leem, J. S. Park, P. Thordarson and J. L. Sessler, *J. Am. Chem. Soc.,* 2015, **137**, 16038-16042.

J. Park, L.-B. Sun, Y.-P. Chen, Z. Perry and H.-C. Zhou, *Angew. Chem. Int. Ed.,* 2014, **53**, 5842-5846.

S. K. Samanta, J. Quigley, B. Vinciguerra, V. Briken and L. Isaacs, *J. Am. Chem. Soc.,* 2017, **139**, 9066-9074.

K. Nakabayashi, M. Kawano and M. Fujita, *Angew. Chem. Int. Ed.,* 2005, **44**, 5322-5325.

K. Yazaki, S. Noda, Y. Tanaka, Y. Sei, M. Akita and M. Yoshizawa, *Angew. Chem. Int. Ed.,* 2016, **55**, 15031-15034.

S. Bivaud, J.-Y. Balandier, M. Chas, M. Allain, S. Goeb and M. Sallé, *J. Am. Chem. Soc.,* 2012, **134**, 11968-11970.

V. Croué, S. Goeb and M. Sallé, *Chem. Commun.,* 2015, **51**, 7275-7289.

M. Yamashina, Y. Sei, M. Akita and M. Yoshizawa, *Nat. Commun.,* 2014, **5**, 4662.

D. Samanta, D. Galaktionova, J. Gemen, L. J. W. Shimon, Y. Diskin-Posner, L. Avram, P. Král and R. Klajn, *Nat. Commun.,* 2018, **9**, 641.

L.-X. Cai, S.-C. Li, D.-N. Yan, L.-P. Zhou, F. Guo and Q.-F. Sun, *J. Am. Chem. Soc.,* 2018, **140**, 4869-4876.

J. L. Bolliger, A. M. Belenguer and J. R. Nitschke, *Angew. Chem. Int. Ed.,* 2013, **52**, 7958-7962.

O. Satu, J. Tao and Y.-Z. Zhang, *Angew. Chem. Int. Ed.*, 2007, **46**, 2152-2187.

T. Liu, H. Zheng, S. Kang, Y. Shiota, S. Hayami, M. Mito, O. Sato, K. Yoshizawa, S. Kanegawa and C. Duan, *Nat. Commun.,* 2013, **4**, 2826.

O. Sato, *Nat. Chem.,* 2016, **8**, 644-656.

J. A. DeGayner, I.-R. Jeon, L. Sun, M. Dincă and T. D. Harris, J. Am. Chem. Soc., 2017, 139, 4175-4184.

H.-Y. Li, Y.-L. Wei, X.-Y. Dong, S.-Q. Zang and T. C. W. Mak, *Chem. Mater.,* 2015, **27**, 1327-1331.

Q. Sui, P. Li, N.-N. Yang, T. Gong, R. Bu and E.-Q. Gao, *ACS Appl. Mater. Int.,* 2018, **10**, 11056-11062.

S. Goeb, S. Bivaud, P. I. Dron, J.-Y. Balandier, M. Chas and M. Sallé, *Chem. Commun.,* 2012, **48**, 3106-3108.

Y. Liu, W. Zhao, C.-H. Chen and A. H. Flood, *Science,* 2019, **365**, 159-161.

C. Kahlfuss, T. Gibaud, S. Denis-Quanquin, S. Chowdhury, G. Royal, F. Chevallier, E. Saint-Aman and C. Bucher, *Chem. – Eur. J.* 2018, **24**, 13009-13019.

A. Iordache, M. Oltean, A. Milet, F. Thomas, B. Baptiste, E. Saint-Aman and C. Bucher, *J. Am. Chem. Soc.,* 2012, **134**, 2653-2671.

D. P. August, G. S. Nichol and P. J. Lusby, *Angew. Chem. Int. Ed.,* 2016, **55**, 15022-1502.

D. Yang, J. Zhao, L. Yu, X. Lin, W. Zhang, H. Ma, A. Gogoll, Z. Zhang, Y. Wang, X.-J. Yang and B. Wu, *J. Am. Chem. Soc.,* 2017, **139**, 5946-5951.

D. Preston, S. M. McNeil, J. E. M. Lewis, G. I. Giles and J. D. Crowley, *Dalton Trans.,* 2016, **45**, 8050-8060.
G. Pognon, C. Boudon, K. J. Schenk, M. Bonin, B. Bach and J. Weiss, *J. Am. Chem. Soc.,* 2006, **128**, 3488-3489.
S. Demir, J. M. Zadrozny, M. Nippe and J. R. Long, *J. Am. Chem. Soc.,* 2012, **134**, 18546-18549.
E. M. Fatila, M. Rouzières, M. C. Jennings, A. J. Lough, R. Clérac and K. E. Preuss, *J. Am. Chem. Soc.,* 2013, **135**, 9596-9599.
G. Brunet, M. Hamwi, M. A. Lemes, B. Gabidullin and M. Murugesu, *Commun. Chem.,* 2018, **1**, 88.
B. S. Dolinar, S. Gómez-Coca, D. I. Alexandropoulos and K. R. Dunbar, *Chem. Commun.,* 2017, **53**, 2283-2286.
C. Kahlfuss, S. Denis-Quanquin, N. Calin, E. Dumont, M. Garavelli, G. Royal, S. Cobo, E. Saint-Aman and C. Bucher, *J. Am. Chem. Soc.,* 2016, **138**, 15234−15242.
C. Kahlfuss, A. Milet, J. Wytko, J. Weiss, E. Saint-Aman and C. Bucher, *Org. Lett.,* 2015, **17**, 4058-4061.
K. Moon, J. Grindstaff, D. Sobransingh and A. E. Kaifer, *Angew. Chem. Int. Ed.,* 2004, **43**, 5496-5499.
L. Zhang, T.-Y. Zhou, J. Tian, H. Wang, D.-W. Zhang, X. Zhao, Y. Liu and Z.-T. Li, *Polym. Chem.,* 2014, **5**, 4715-4721.
G. Das, T. Prakasam, S. Nuryyeva, D. S. Han, A. Abdel-Wahab, J.-C. Olsen, K. Polychronopoulou, C. Platas-Iglesias, F. Ravaux, M. Jouiad and A. Trabolsi, *J. Mater. Chem. A,* 2016, **4**, 15361-15369.
H. D. Correia, S. Chowdhury, A. P. Ramos, L. Guy, G. J.-F. Demets and C. Bucher, *Polym. Int.,* 2019, **68**, 572-588.
L. Striepe and T. Baumgartner, *Chem. – Eur. J.,* 2017, **23**, 16924-16940.
Y. Wang, M. Frasconi and J. F. Stoddart, *ACS Cent. Sci.,* 2017, **3**, 927-935.
A. R. Pease, J. O. Jeppesen, J. F. Stoddart, Y. Lio, C. P. Collier and J. R. Heath, *Acc. Chem. Res.,* 2001, **34**, 433-444.
M. A. Lemes, G. Brunet, A. Pialat, L. Ungur, I. Korobkov and M. Murugesu, *Chem. Commun.,* 2017, **53**, 8660-8663.
M. A. Lemes, H. N. Stein, B. Gabidullin, K. Robeyns, R. Clérac and M. Murugesu, *Chem. – Eur. J.,* 2018, **24**, 4259-4263.
D. Casanova, M. Llunell, P. Alemany and S. Alvarez, *Chem. – Eur. J.,* 2005, **11**, 1479-1494.
A. L. Spek, *Acta Crystallogr. Sect. C*, 2015, **71**, 9-18.
X.-Y. Lv, M.-S. Wang, C. Yang, G.-E. Wang, S.-H. Wang, R.-G. Lin and G.-C. Guo, *Inorg. Chem.,* 2012, **51**, 4015-4019.
C. Sun, G. Xu., X.-M. Jiang, G.-E. Wang, P.-Y. Guo, M.-S. Wang and G.-C. Guo, *J. Am. Chem. Soc.,* 2018, **140**, 2805-2811.
N. Leblanc, M. Allain, N. Mercier and L. Sanguinet, *Cryst. Growth Des.,* 2011, **11**, 2064-2069.
J.-K. Sun, P. Wang, C. Chen, X.-J. Zhou, L.-M. Wu, Y.-F. Zhang and J. Zhang, *Dalton Trans.,* 2012, **41**, 13441-13446.
J.-J. Liu, Y.-F. Guan, M.-J. Lin, C.-C. Huang, W.-X. Dai, *Cryst. Growth Des.,* 2016, **16**, 2836-2842.
F. Wan, L.-X. Qiu, L.-L. Zhou, Y.-Q. Sun and Y. You, *Dalton Trans.* 2015, **44**, 18320-18323.
T. P. Le, J. E. Rogers and L. A. Kelly, *J. Phys. Chem. A,* 2000, **104**, 6778-6785.
O. Toma, M. Leroux, N. Mercier, M. Allain, A. H. Kassiba, S. K. K. Swamy, J. Dittmer, *Eur. J. Inorg, Chem.,* 2016, **7**, 1036-1043.
W. W. Porter and T. P. Vaid, *J. Org. Chem.,* 2005, **70**, 5028-5035.
Q. Sui, X.-T. Ren, Y.-X. Dai, K. Wang, W.-T. Li, T. Gong, J.-J. Fang, B. Zou, E.-Q. Gao and L. Wang, *Chem. Sci.* 2017, **8**, 2758-2768.
R. Sure and S. Grimme, *J. Comput. Chem.,* 2013, **34**, 1672-1685.
F. Neese, *Wiley Interdiscip. Rev.: Comput. Mol. Sci.*, 2012, **2**, 73-78.
J.-K. Sun, P. Wang, Q.-X. Yao, Y.-J. Chen, Z.-H. Li, Y.-F. Zhang, L.-M. Wu and J. Zhang, *J. Mater. Chem.,* 2012, **22**, 12212-12219.
L. A. Vermeulen and M. E. Thompson, *Nature,* 1992, **358**, 656-658.
N. Ishikawa, M. Sugita, T. Ishikawa, S. Koshihara and Y. Kaizu, *J. Am. Chem. Soc.*, 2003, **125**, 8694-8695.
M. A. AlDamen, J. M. Clemente-Juan, E. Coronado, C. Martí-Gastaldo and A. Gaita-Ariño, *J. Am. Chem. Soc.,* 2008, **130**, 8874-8875.
N. Ishikawa, M. Sugita and W. Wernsdorfer, *Angew. Chem. Int. Ed.,* 2005, **44**, 2931-2935.
G.-J. Chen, C.-Y. Gao, J.-L. Tian, J. Tang, W. Gu, X. Liu, S.-P. Yan, D.-Z. Liao and P. Cheng, *Dalton Trans.*, 2011, **40**, 5579-5583.
S.-D. Jiang, B.-W. Wang, G. Su, Z.-M. Wang and S. Gao, *Angew. Chem. Int. Ed.,* 2010, **49**, 7448-7451.
J. J. Baldoví, J. J. Borrás-Almenar, J. M. Clemente-Juan, E. Coronado and A. Gaita-Ariño, *Dalton Trans.,* 2012, **41**, 13705-13710.
J.-L. Liu, Y.-C. Chen and M.-L. Tong, *Chem. Soc. Rev.,* 2018, **47**, 2431-2453.
H. Chen, G. Zheng, M. Li, Y. Wang, Y. Song, C. Han, J. Dai and Z. Fu, *Chem. Commun.*, 2014, **50**, 13544-13546.
G. Xu, G.-C. Guo, M.-S. Wang, Z.-J. Zhang, W.-T. Chen and J.-S. Huang, *Angew. Chem. Int. Ed.,* 2007, **46**, 3249-3251.
J.-K. Sun, L.-X. Cai, Y.-J. Chen, Z.-H. Li and J. Zhang, *Chem. Commun.,* 2011, **47**, 6870-6872.

D.-F. Shen, S. Li, H. Liu, W. Jiang, Q. Zhang and G.-G. Gao, *J. Mater. Chem. C,* 2015, **3**, 12090-12097.
Y.-Q. Sun, F. Wan, X.-X. Li, J. Lin, T. Wu, S.-T. Zheng and X. Bu, *Chem. Commun.,* 2016, **52**, 10125-10128.
W. Yang, H.-R. Tian, J.-P. Li, Y.-F. Hui, X. He, J. Li, S. Dang, Z. Xie and Z.-M. Sun, *Chem. – Eur. J.,* 2016, **22**, 15451-15457.
E. E. Méndez, C. Crespo-Hernández, R. Figueroa, R. Arce and E. Quiñones, *J. Photochem. Photobiol. A,* 2001, **142**, 19-24.
J. -J. Liu, Y.-F. Guan, M.-J. Lin, C.-C. Huang and W.-X. Dai, *Cryst. Growth Des.,* 2015, **15**, 5040-5046.